Photoprogrammable Circularly Polarized Phosphorescence Switching of Chiral Helical Polyacetylene Thin Films

Zizhao Huang, Zhenyi He, Bingbing Ding, He Tian and Xiang Ma*

Author Information

Key Laboratory for Advanced Materials and Feringa Nobel Prize Scientist Joint Research Center, Frontiers Science Center for Materiobiology and Dynamic Chemistry, Institute of Fine Chemicals, School of Chemistry and Molecular Engineering, East China University of Science and Technology, Meilong Road 130, Shanghai 200237, P. R. China

Zizhao Huang, Zhenyi He, Bingbing Ding, He Tian and Xiang Ma

Abstract

The developments of pure organic room-temperature phosphorescence (RTP) materials with circularly polarized luminescence (CPL) have significantly facilitated the future integration and systemization of luminescent material in fundamental science and technological applications. Herein, a new type of photoinduced circularly polarized RTP materials was constructed by homogeneously dispersing phosphorescent chiral helical substituted polyacetylenes into a processable poly(methyl methacrylate) (PMMA) matrix. This substituted polyacetylenes play vital roles in the propagation of CPL and present prominently optical characteristics with high absorption and luminescent dissymmetric factors up to 0.029 (g_{abs}) and 0.019 (g_{lum}). The oxygen consumption properties of PMMA films under UV light irradiation endowed materials with dynamic chiro-optical functionality, which can leverage of light to precisely control and manipulate the circularly polarized RTP properties with the remarkable advantages of being contactless, wireless and fatigue-resistant. Significantly, the distinct materials with dynamic properties can be used as novel anti-counterfeiting materials involving photoprogrammability.

Introduction

Purely organic emitting materials with room-temperature phosphorescence (RTP), featuring large Stokes shifts, long-lived emission and favorable processability, have been a thriving topic in bioimaging[1,2], sensors[3-5], anti-counterfeiting materials[6-8] and so forth[9-11]. Amongst the many possibilities in molecular design for RTP materials production, systematical investigation of molecular functions and material properties anchoring on chirality manipulate would be a scientifically frontier research[12-15]. To date, exponential attention have been paid to the design and fabrication of organic optoelectronic materials with circularly polarized luminescence (CPL) functionality[16-22], and several successful examples of circularly polarized room-temperature phosphorescent materials were designed by confining the motions of chiral aromatic molecules in the rigid crystals or polymers[23-27]. However, circularly polarized RTP materials with responsiveness to internal factors or external environment stimuli are still rarely reported[28], especially those with favorable practicability. This is primarily for the reason that while crystal engineering is a frequently used strategy to provide protective and rigid environments to induce RTP emission, it is probably limited in flexible design and physiological applications. Also, until now no efficient design strategies have been presented and discussed. Therefore, if stimulus-responsive circularly polarized RTP materials can be exploited, the change in chiro-optical property under external stimulus could be employed as another visual monitoring parameter in addition to luminescence lifetime and color in phosphorescence, which will necessarily contribute to their practical application.

More recently, our group constructed independently circularly polarized RTP emission in an amorphous state by attaching axial chiral phosphors into polyacrylamide chains[29]. However, while the amorphous polymers with robust hydrogen bonding networks endowed the materials with high RTP quantum yield, they also limited its stimulus-response and sensitivity. Hence, to overcome the limitation and promote the application prospects of polymer-based organic circularly polarized RTP materials in stimulating corresponding materials, we considered the modification of the rigidification in the polymer network to precisely control the photoresponsiveness. Accordingly, we conveniently developed chiral polymers containing single-handed helical structures using the copolymerization of chiral phNA and phosphorescent BrNpA, we developed chiral polymers comprising single-handed helical construction conveniently by taking advantage of copolymerization of chiral phNA and phosphor BrNpA. By intentionally introducing these chiral helical polymers into the polymethyl methacrylate (PMMA) matrix, the flexible films with potential circularly polarized phosphorescence emission were obtained from molding implantation. The unambiguously helical construction played an essential role in the propagation of circularly polarized light and exhibited room-temperature phosphorescence with remarkable handedness. Besides, the oxygen consumption characteristics of PMMA under UV light irradiation endowed materials with dynamic chiro-optical functionality that facilitate the control and modulation of the circularly polarized RTP properties non-invasively by light. Such photoresponsive chiral materials are considered prominent candidates for the utilization in stimulus-controllable chiroptical devices with high-optical efficiency and stabilized optical properties.

Results

The formation of chiral thin films. As illustratively shown in Figure 1a, the chiral polymer was constructed from chiral 4-isobutylphenyl-N-propanamide derivative (phNA) and the RTP chromophore 4-bromo-1,8-naphthalimide derivative (BrNpA) directly by the copolymerization in the presence of rhodium-based catalyst. The obtained chiral p(phNA-co-BrNpA) copolymer was analyzed by FT-IR spectroscopy and gel permeation chromatography (GPC) (Figure S2 and Table S1, Supporting Information). The successful polymerization of phNA with BrNpA can be demonstrated by the disappearance of vibrational absorption peak at about 2114 cm^{-1} from FT-IR spectra, which belongs to the symbolic absorption peak of C≡C group. The GPC measurement of the obtained copolymers with different phNA/BrNpA molar ratios were listed in Table S1, which the results of moderate number-average molecular weight (Mn) and narrow molecular weight distribution (Mw/Mn) further convincingly confirmed the successful copolymerization. Besides, the actual copolymer composition was calculated by ^1H NMR spectra. For an example shown in Figure S3, p($phNA_7BrNpA_3$) was calculated to be 7:3.64, which corresponded to the theoretical value (7:3 in mol). All of the above results indicate that the required copolymers were obtained efficiently.

However, the weakly rigid environment construct by chiral polyacetylenes were difficult to inhibit both the nonradiative deactivation of the excited triplet state and oxygen quenching by blocking the oxygen diffusion into the rigid matrix well enough, only extremely weak room-temperature phosphorescent emission was obtained (Figure S6). To furnish a relatively rigid environment for the chiral copolymer, the flexible p(phNA-co-BrNpA)-PMMA film with intermolecular hydrogen bonding was subsequently prepared accordingly through dissolving p(phNA-co-BrNpA) into polymethyl methacrylate (PMMA) used as a matrix. The distinct photoinduced RTP emission could be discovered form the p(phNA$_7$BrNpA$_3$)-PMMA film, from practically non-RTP emission to the intense emission with a lifetime of 6.08 ms under continuous UV irradiation, while fluorescence emission was unaffected by the UV irradiation, indicating the important role of polymer matrix in phosphorescence effect. (Figure 1c, S7). For this phenomenon, the dominant factor may be the consumption of oxygen in the PMMA matrix under continuous UV irradiation, since oxygen molecules present an unusual triplet ground state, which can interact with triplet excitons and quench them (Figure 1d). Besides, to exclude the effect of the PMMA film thickness on the activation of RTP, we varied the phNA/BrNpA weight ratio in the p(phNA-co-BrNpA)-PMMA from 5/5 to 6/4, 7/3 and 8/2, giving four films with similar thickness around 225 mm (Figure S5).

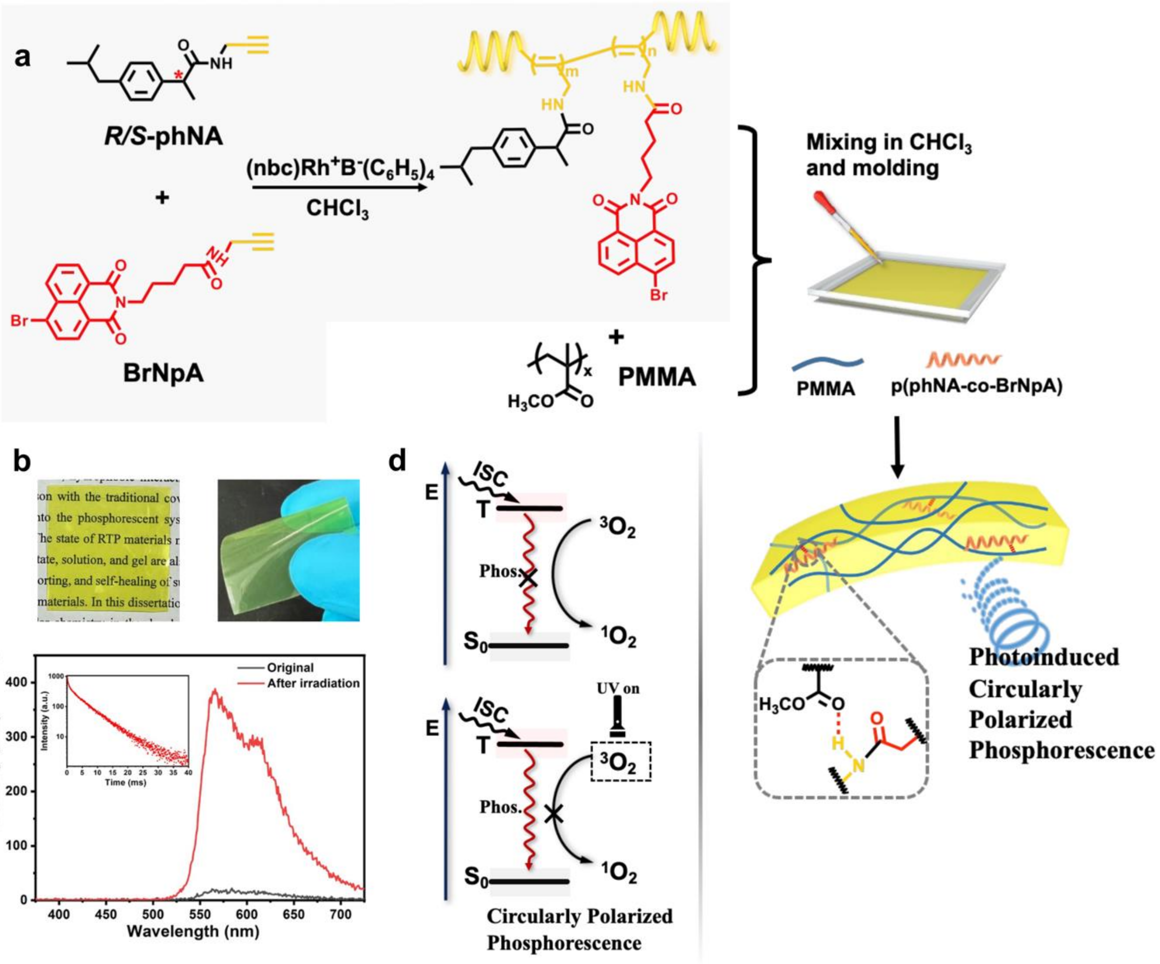

Figure 1. **a** Schematic illustration of the structure and preparation of the p(phNA-co-BrNpA)-PMMA film. A flexible p(phNA-co-BrNpA) copolymer with amide group interacted with PMMA to form hydrogen bonding crosslinked network. **b** Photographs of the PMMA composite film. The films were flexible and could be bent. **c** Gated emission spectra of p(phNA$_7$BrNpA$_3$)-PMMA. Inset shows the phosphorescence decay curves (λ_{ex}=365 nm, delay time=0.1 ms). **d** Energy diagram and performance characterization of oxygen consumption in film.

Photoinduced RTP behavior. Expectantly, the photophysical properties of the p(phNA-co-BrNpA)-PMMA film were systematically investigated. p(*R*-phNA$_7$BrNpA$_3$)-PMMA was picked out as the representative for the following elaboration. As shown in the photoluminescence spectra and the corresponding photographs, the RTP emission located at 586 nm of this film was negligible at initial state, while significantly enhanced upon continuous UV irradiation at ambient conditions. After the films were ceased UV irradiation and exposed to atmospheric conditions, triplet oxygen could permeate into the film and cause phosphorescence quenching (Figure 2a and Movie S1). Other films with different phNA/BrNpA copolymerization molar ratios exhibited approximately the same phenomenon (Figure S8). We next verified the stability of the observed phosphorescence photoswitching performance, as shown in Figure 2d, the remarkably stable phosphorescent performance was demonstrated by the turning-on and -off repeated cycles of UV-irradiation, which has possibilities for extensive and advanced applications in many fields. Considering the diversity of application scenarios, we quantitatively investigated the influence of photoinduced RTP behavior in different power UV light. Impressively, the more easily activated RTP can be observed in higher power density of the UV lamp, which means that a greater degree of phosphorescence emission enhancement could be achieved through UV light induction in a short period of time (Figure 2e).

To investigate the relationship between copolymerization molar ratios of the copolymer and the photoinduced RTP properties, we characterized the absolute quantum yields of the films, indicating that the quantum yields intensity increase and then decline with the amplification of the molar ratios of phNA/BrNpA in copolymer (Figure 2f). This could be explained by the aggregation of phosphor at low phNA/BrNpA molar ratios leading to luminescence quenching, while at increasing phNA/BrNpA molar ratios, the UV-vis absorption increases leading to enhanced self-absorption. We next investigated the loading-dependent oxygen permeability of the p(phNA-co-BrNpA)-PMMA with different phNA/BrNpA ratio via monitoring fade-away process of the real-time RTP quantum yield after ceasing UV irradiation. As shown in Figure 2g, the site-resistant isobutyl group in phNA furnishes relatively steric hindrance, contributed to a steric vacancy in the physical entanglement between the polymer chains, which affects the denseness of the polymer chains and thus diminishes the rigidification effect on the phosphorescent moieties. This steric hindrance may also enhance the possibility of oxygen diffusion and permeability, hence the thin films with higher phNA/BrNpA ratios evidently presented a shorter retention time.

Contrastingly, shorter retention time were observed for PMMA films prepared by direct doping p(phNA) with BrNpA.

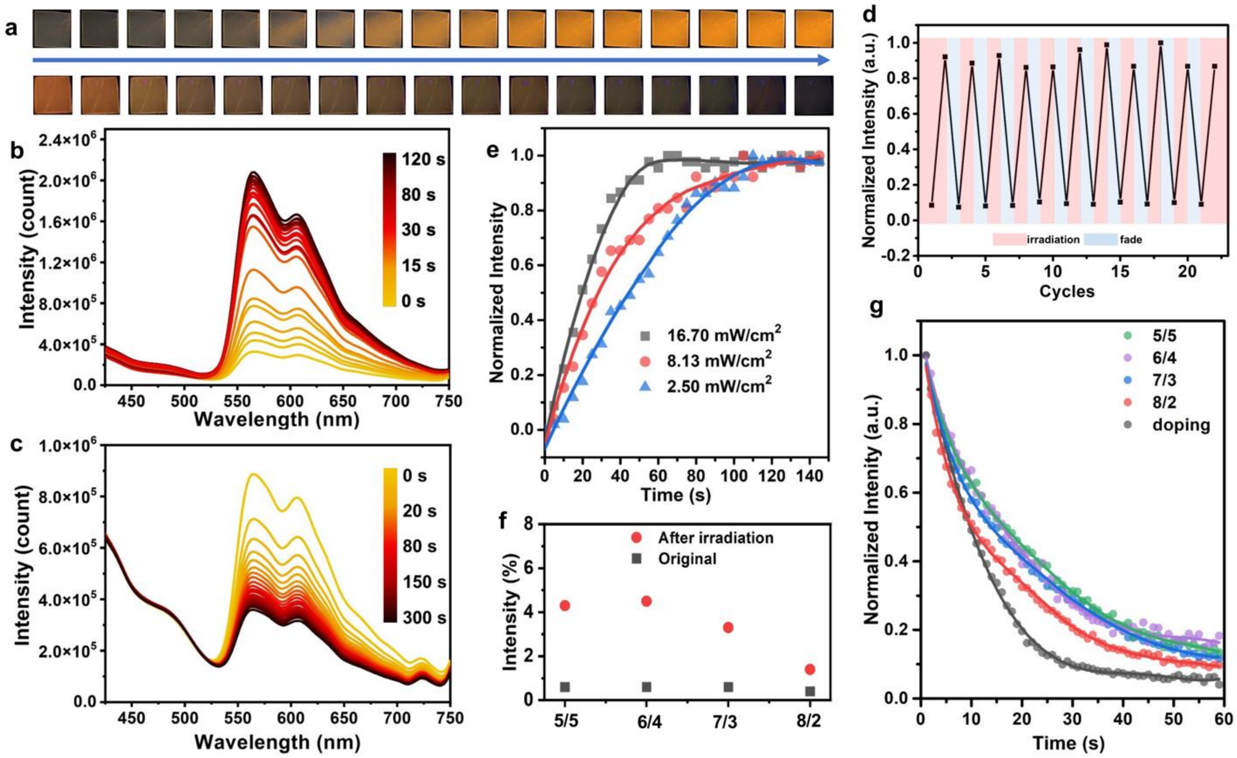

Figure 2. a Photographic image series of p(phNA$_7$BrNpA$_3$)-PMMA under continuous UV light irradiation (up) and after ceasing irradiation (bottom). The photoluminescence spectra of p(phNA$_7$BrNpA3)-PMMA under **b** sustaining UV light irradiation and **c** after ceasing irradiation (λ_{ex}=365 nm). **d** The turning-on and -off repeated cycles of the p(phNA$_7$BrNpA$_3$)-PMMA film. **e** Time-dependent normalized phosphorescence intensity of p(phNA$_7$BrNpA$_3$)-PMMA under UV irradiation with different power densities. **f** Quantum yield changes of p(phNA-co-BrNpA)-PMMA films with different copolymerization molar ratios before and after UV irradiation. **g** Time-dependent normalized phosphorescence quantum yield of p(phNA$_7$BrNpA$_3$)-PMMA with different copolymerization molar ratios after ceasing irradiation.

Photoinduced chiro-optical characteristic. After confirming the copolymerization and photoinduced RTP performance of the polymers films, the circular dichroism (CD) and circularly polarized luminescence (CPL) were employed to further analyze their helical conformation. The p(*R/S*-phNA-co-BrNpA) presented intense mirror-CD signals near 425 nm in both THF and PMMA films, which demonstrated the preferred-handed helical structures of the backbones of polyacetylene (Figure 3b, S9, S10). Furthermore, the intensity of CD signals enhanced significantly with the increment of *R/S*-phNA ratio in the copolymer, which was attributed to the increase in the proportion of chiral monomers during the polymerization process to improve the optical activity, and further demonstrated by the g_{abs} values (Figure 3e). Apparently, the polymers films lacking chiral monomers phNA cannot form a predominant singlehanded helix under suitable circumstances (Figure S12).

CPL reflects the excited state properties of chiral materials. However, it should be mentioned that chirality and luminescence are not sufficient conditions for CPL, and it is frequent for chiral luminescent materials not to possess CPL properties, mainly due to the complexity of the chiral transfer process[30,31]. Excitingly, the CPL intensity of p(*R/S*-phNA-co-BrNpA)-PMMA film dramatically enhanced with the UV irradiation, and would return to the initial state after 5-6 min of standing under natural conditions, showing the reversible photoresponsive CPL effect, which exhibited a similar tendency with photoluminescence spectra (Figure 3a, S13, S14). Ascribing to the changeless of polymer composition and conformation during the phosphorescence switching process, the dissymmetric factor g_{lum}, quantified the extent of chiral dissymmetry in luminescence, does not alter during this process. Besides, the increasement of phNA/BrNpA copolymerization molar ratios can improve the optical activity and thus the g_{lum}， and the maximum g_{lum} can be obtained at 1.86×10^{-2} (Figure 3c). Correspondingly, the polymer-PMMA films lacking chiral monomers phNA or phosphor BrNpA cannot exhibit CPL properties (Figure S15). As influenced by the strong excitation light source of the CPL spectra instrument, we shorten the spectral scanning wavelength range and sped up the scanning speed to investigate the CPL decay rate of different phNA/BrNpA copolymerization molar ratios (Figure S16). As shown in figure 3d, the decay law of CPL spectrum was the same as the photoluminescence spectra. A large g_{lum} indicates well-polarized purity of the emission, while the quantum yield (PLQY) is also an essential parameter to evaluate comprehensive performance of CPL-active materials. Hence, we can propose the multiplication of the dissymmetry factor and the PLQY as a figure of merit (FM = g_{lum}×PLQY) for evaluating the CPL property[32]. As shown in Figure 3e, the highest FM value of 4.9×10^{-3} exhibited the potential of chiral helical substituted polyacetylene in high-efficiency circularly polarized RTP materials, although there is still a long way to reach high FM values.

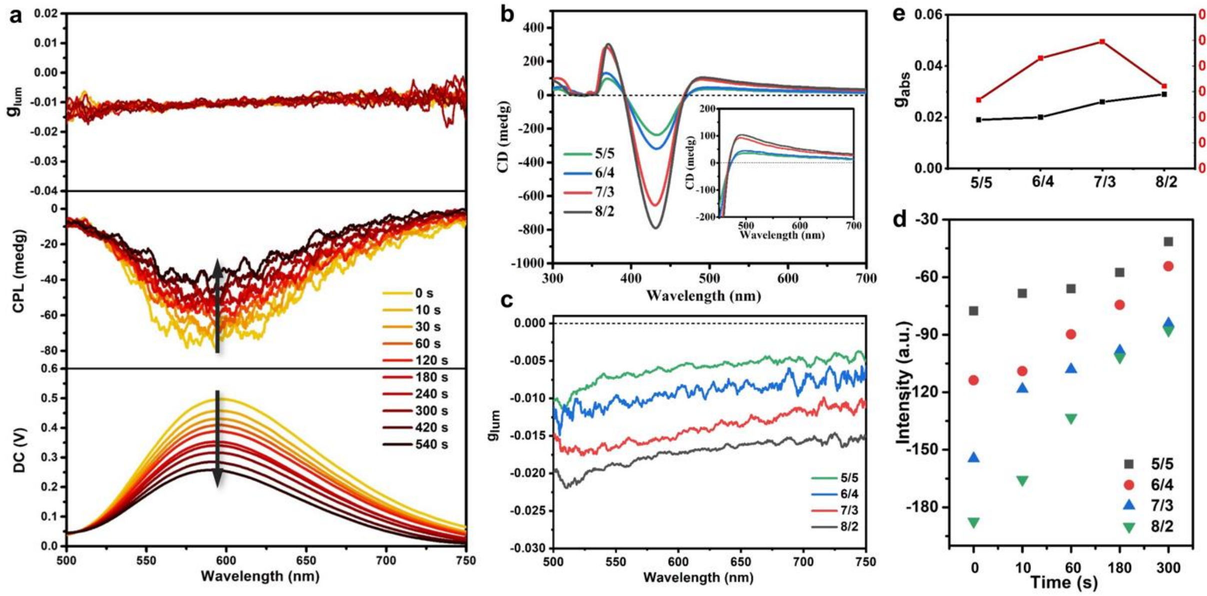

Figure 3. a The CPL of p(R-phNA$_7$BrNpA$_3$)-PMMA film during fade-away process (λ_{ex}=365 nm). **b** The CD spectra of p(R-phNA-co-BrNpA)-PMMA film with different copolymerization molar ratios. **c** The g_{lum} spectra of p(R-phNA-co-BrNpA)-PMMA film with different copolymerization molar ratios. **d** Time-dependent normalized CPL intensity (at 583 nm) of p(R-phNA-co-BrNpA)-PMMA with different copolymerization molar ratios after ceasing irradiation (according to Figure S16). **e** The g_{abs} and FM value of p(R-phNA-co-BrNpA)-PMMA film with different copolymerization molar ratios.

The mechanism for photoinduced circularly polarized RTP properties. The underlying origination of these unique photoinduced RTP effect and distinct CPL properties were explored. The phosphor BrNpA in the ground state (S_0) absorbed the photons was excited to S_1 state under UV irradiation, and then to the T_1 through ISC transition. However, the highly reactive nonradiative energy transfer from the triplet state of the phosphor to triplet oxygen could lead to the quenching of phosphorescence[33-36]. After a sustaining UV irradiation over a period of time to consume the dissolved oxygen in PMMA film, then the triplet excitons could decay as phosphorescence rather than being quenched by oxygen molecules, thus producing the photoinduced RTP characteristic (Figure 4c). To confirm the existence of a similar mechanism, the surrounding atmospheric influence on photoinduced RTP emission was investigated in nitrogen and oxygen environment, respectively. As shown in Figure 4a and S18, the p(phNA$_7$BrNpA$_3$)-PMMA film was placed in cuvette with a needle which can inject nitrogen or oxygen into the system. The film exhibited non-RTP emission even after continuous UV irradiation when the tube was kept oxygen-filled. Contrastively, the film could give a promptly response RTP to UV irradiation after replenished the tube with nitrogen. In addition, it is generally recognized that polyvinyl alcohol (PVA) possesses abundant hydrogen bonding network that prevents the phosphor from oxygen[37,38]. Therefore, we coated a layer of PVA on the surface of the material, and as can be seen from Figure 4b, the material coated with PVA that can isolate oxygen did not exhibit photoactivatied phenomenon. Hence, it is certified that the existence of oxygen plays a significant role in the appearance of dynamic RTP behavior.

Recently, it was demonstrated that chiral helical substituted polyacetylenes can function as handedness-selective fluorescence filters to convert unpolarized fluorescence into circularly polarized luminescence by the fluorescence-selective absorption mechanism when the CD spectrum overlaps with the luminescence spectrum[39-41]. Therefore, to investigate whether the CPL signal of the films was generated because of the handed-selective fluorescence absorption of chiral helical polymers, we constructed the racemic phosphor BrNpA and nonfluorescent chiral polymer p(phNA), respectively, and then prepared them into PMMA films to implement "positioning control" CPL tests. We find that CPL could be detected when two thin films were placed in the order "light source-BrNpA films-p(phNA) film-detector". However, when the positions of the BrNpA film and p(phNA) film were replaced, the CPL signal totally vanished (Figure 4d). This manifested that the relative position between the phosphor and the chiral helical polymer is significant for successful CPL construction. We next simply doped BrNpA and p(phNA) into PMMA to prepare the films and found that they also exhibited CPL properties (Figure S17).

Experimental results indicated the existence of chiral helical polymers is essential for CPL preparation, and the CPL stemmed from the nonfluorescent chiral helical polymers “filter” affection.

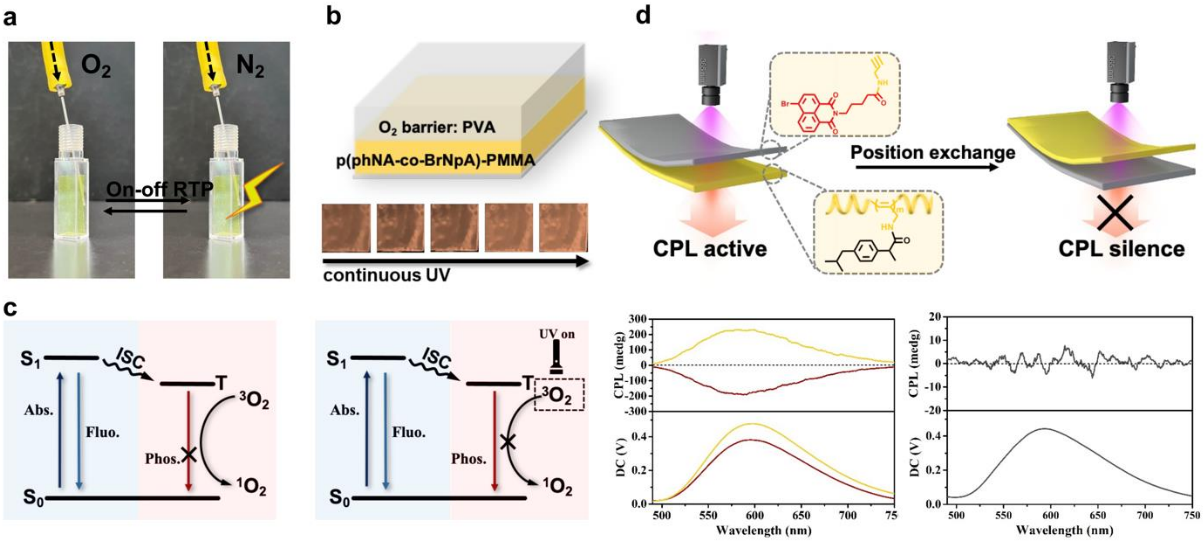

Figure 4. a Nitrogen and oxygen were alternately filled into the quartz tube. p(*R*-phNA$_7$BrNpA$_3$)-PMMA exhibited RTP “turn-on” and “off” under 365 nm UV irradiation. **b** Schematic diagram and photograph of p(phNA-co-BrNpA)-PMMA coated with a layer of PVA. **c** The diagram of the internal mechanism of oxygen consumption under UV irradiation. **d** Schematic diagram of different CPL test methods (up) and the corresponding CPL spectra (bottom). The chiral helical polymers can serve as a “filter” to generate CPL.

Applications of photoprogrammable circularly polarized RTP materials. These versatile luminescent properties and the flexibility and plasticity of the materials enable the construction of advanced smart photonic technologies. Hence, under the UV light irradiation, the formation of the PMMA film can perform the light-printing properties (Figure 5a). Besides, we fabricated the self-erasable transient information storage and anti-counterfeiting in various daily materials by utilizing facile stencil printing with the p(*R/S*-phNA$_7$BrNpA$_3$)-PMMA concentrated solution as paint to generate the information patterns. As presented in Figure 5b, the patterns numbers were invisible under natural light on paper, wood, glass and polyester, which was increasingly uncovered with orange emission under continuous 365 nm UV irradiation. Importantly, while the number "0/5/0/9" exhibited a similar emission color under continuous 365 nm UV irradiation, the positive CPL signal can be observed from the number "0/0", but not from the number "5/9". This provided anti-counterfeiting information involving CPL signal with more application scenarios. In addition, we conveniently prepared the materials into lampshade by adding p(phNA-co-BrNpA)-PMMA $CHCl_3$ suspension to a stencil mask, then drying the suspension and removing the stencil mask. When connected to the power supply and the LED was turned on at 5.5 V, the lampshade placed on the 365 nm commercial LED will gradually light up with bright orange emission. Then we utilize nine small bulbs connected in parallel to form a lamp panel and artificially labeled with numbers. And using different copolymerization molar ratios of the materials to fabricate the lampshades. As shown in Figure 5c and Movie S2, the lampshades will have different times of being illuminated when the lamp panel was connected to the power supply. Therefore, it is possible to detect different digital patterns at different time scales, which can be potentially employed as a time-informed anti-counterfeiting technology.

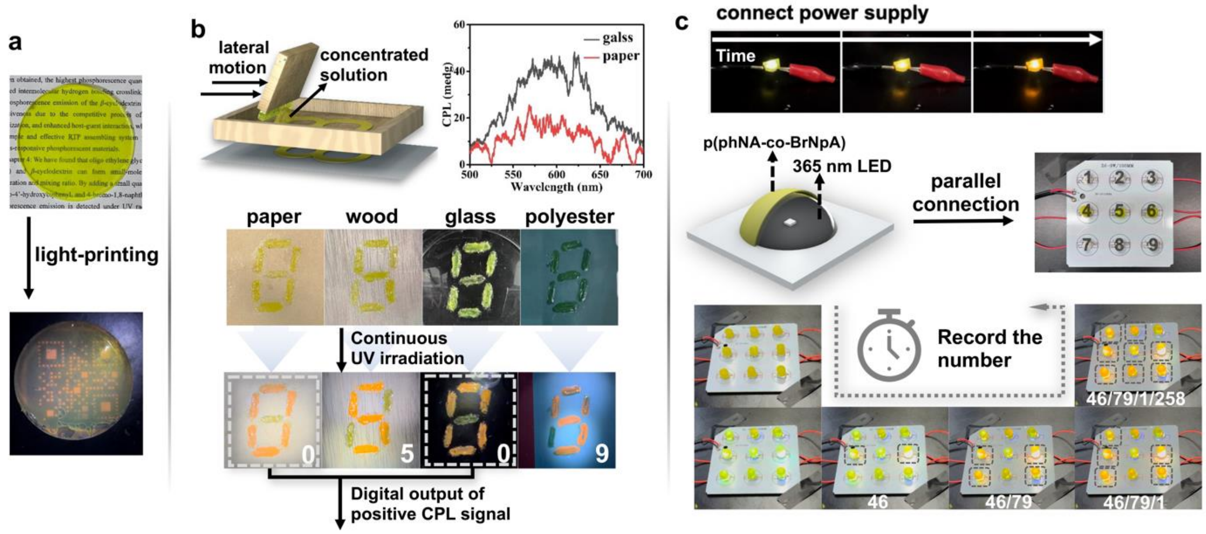

Figure 5. a Photographs of the p(phNA-co-BrNpA)-PMMA with light-printing QR code pattern in front of a photomask under 365 nm light. **b** Manufacturing process of the anti-counterfeiting patterns and the CPL spectrum of the patterns (top). The pattern of "8" was generated on each material using p(phNA)-PMMA first, and the hidden pattern was printed again using p(*R/S*-phNA$_7$BrNpA$_3$)-PMMA. Photographs of hidden pattern taken under UV irradiation (bottom). **c** Photographs of the fabrication

and properties of the smart photoelectric material. When connected to the power supply, record the number corresponding to the lighted bulb as time progresses. First is the number 46, followed by 79, 1 and 258.

Discussion

In summary, we have exploited a new type of photoinduced circularly polarized RTP materials by homogeneously dispersing phosphorescent chiral helical substituted polyacetylenes into an rigid poly(methyl methacrylate) matrix. Benefiting from the chiral polyacetylenes with a predominant singlehanded helix, the flexible films exhibited prominent handedness optical properties. The oxygen consumption characteristics of the concomitant PMMA under UV light irradiation generated significant dynamic chiro-optical modulation involving photoprogrammability, which enriched the functionality of RTP materials. This renders these films competitive candidates for the promising chiro-optical applications with dynamic properties and favorable processability.

Methods

Materials. All reagents and solvents employed were commercially available and used as received without further purification. 4-Bromo-1,8-naphthalic anhydride (Adamas-beta), which was purified by column chromatography (ethyl acetate/cyclohexane, 1/1, v/v). Solvents were purified according to standard laboratory methods. The molecular structures were confirmed using ^{1}H NMR, ^{13}C NMR and high-resolution ESI mass spectroscopy.

General methods. The UV-Vis absorption spectra and PL spectra were performed on a Varian Cray 500 spectrophotometer and a Horiba Fluoromax-4 at 25 °C, respectively. Phosphorescence spectra and phosphorescence lifetimes were obtained on a Varian Cary Eclipse spectrophotometer. Quantum yields were measured by using an integrating sphere on a HAMAMATSU Quantaurus-QY C11347-11. Powder X-ray diffraction (XRD) was performed on a D/max2550VB/PC. Circular dichroism (CD) spectra were acquired using the JASCO J815 spectrophotometer. CPL spectra were acquired using the JASCO CPL-200 spectrofluoropolarimeter. GPC was performed on a Series 200.

Contributions

Z. H. and X. M. conceived the project and designed the molecules. Z. H. performed the compound syntheses and characterizations. Z. H., X. M. and H.T. wrote the manuscript. All authors discussed the results and commented on the manuscript.

Corresponding author

Xiang Ma: maxiang@ecust.edu.cn; 0000-0002-8679-4491

Data Availability

All relevant data that support the findings are available within this article and supporting information and are also available from authors upon reasonable request.

Acknowledgements

We gratefully acknowledge the financial support from the National Natural Science Foundation of China (21788102, 22125803, 22020102006, and 21871083), project support by the Shanghai Municipal Science and Technology Major Project (Grant No.2018SHZDZX03), Program of Shanghai Academic/Technology Research Leader (20XD1421300), 'Shu Guang' project supported by Shanghai Municipal Education Commission and Shanghai Education Development Foundation (19SG26), and the Fundamental Research Funds for the Central Universities.

Ethics declarations

The authors declare no competing interests.

References

1. Wang, J., Huang, Z., Ma, X. & Tian, H. Visible-Light-Excited Room-Temperature Phosphorescence in Water by Cucurbit[8]uril-Mediated Supramolecular Assembly. *Angew. Chem. Int. Ed.* **59**, 9928-9933 (2020).

2. Zhou, W.L., *et al.* Ultralong purely organic aqueous phosphorescence supramolecular polymer for targeted tumor cell imaging. *Nat. Commun.* **11**, 4655 (2020).
3. Yao, X., *et al.* Room-Temperature Phosphorescence Enabled through Nacre-Mimetic Nanocomposite Design. *Adv. Mater.* **33**, e2005973 (2021).
4. Liu, X.Q., *et al.* Monochromophore-Based Phosphorescence and Fluorescence from Pure Organic Assemblies for Ratiometric Hypoxia Detection. *Angew. Chem. Int. Ed.* **59**, 23456-23460 (2020).
5. Yuan, Z., *et al.* Methanol Dynamically Activated Room-Temperature Phosphorescence from a Twisted 4-Bromobiphenyl System. *CCS Chem.* **2**, 158-167 (2020).
6. Zhang, X., *et al.* Ultralong phosphorescence cellulose with excellent anti-bacterial, water-resistant and ease-to-process performance. *Nat. Commun.* **13**, 1117 (2022).
7. Li, D., *et al.* Completely aqueous processable stimulus responsive organic room temperature phosphorescence materials with tunable afterglow color. *Nat. Commun.* **13**, 347 (2022).
8. Gu, L., *et al.* Colour-tunable ultra-long organic phosphorescence of a single-component molecular crystal. *Nat. Photonics* **13**, 406-411 (2019).
9. Kashida, J., *et al.* An Air- and Water-Stable B4 N4 -Heteropentalene Serving as a Host Material for a Phosphorescent OLED. *Angew. Chem. Int. Ed.* **60**, 23812-23818 (2021).
10. Chen, B., *et al.* An Organic Host-Guest System Producing Room-Temperature Phosphorescence at the Parts-Per-Billion Level. *Angew. Chem. Int. Ed.* **60**, 16970-16973 (2021).
11. Zhao, W., He, Z. & Tang, B.Z. Room-temperature phosphorescence from organic aggregates. *Nat. Rev. Mater.* **5**, 869-885 (2020).
12. Nitti, A. & Pasini, D. Aggregation-Induced Circularly Polarized Luminescence: Chiral Organic Materials for Emerging Optical Technologies. *Adv. Mater.* **32**, e1908021 (2020).
13. Huang, Z. & Ma, X. Tailoring Tunable Luminescence via Supramolecular Assembly Strategies. *Cell Rep. Phys. Sci.* **1**, 100167 (2020).
14. Zhao, T., Han, J., Duan, P. & Liu, M. New Perspectives to Trigger and Modulate Circularly Polarized Luminescence of Complex and Aggregated Systems: Energy Transfer, Photon Upconversion, Charge Transfer, and Organic Radical. *Acc. Chem. Res.* **53**, 1279-1292 (2020).
15. Zhang, X., Yin, J. & Yoon, J. Recent advances in development of chiral fluorescent and colorimetric sensors. *Chem. Rev.* **114**, 4918-4959 (2014).
16. Zhang, M.M., *et al.* AIE Triggers the Circularly Polarized Luminescence of Atomically Precise Enantiomeric Copper(I) Alkynyl Clusters. *Angew. Chem. Int. Ed.* **59**, 10052-10058 (2020).
17. Takaishi, K., Iwachido, K. & Ema, T. Solvent-Induced Sign Inversion of Circularly Polarized Luminescence: Control of Excimer Chirality by Hydrogen Bonding. *J. Am. Chem. Soc.* **142**, 1774-1779 (2020).
18. Kim, M., Lee, H., Snipes, R.T., Han, M.J. & Tsukruk, V.V. Co-Assembly of Biosynthetic Chiral Nematic Adhesive Materials with Dynamic Polarized Luminescence. *Small* **18**, e2104340 (2022).
19. Yang, Y., da Costa, R.C., Fuchter, M.J. & Campbell, A.J. Circularly polarized light detection by a chiral organic semiconductor transistor. *Nat. Photonics* **7**, 634-638 (2013).
20. Cheng, Q., Hao, A. & Xing, P. A chemosensor-based chiral coassembly with switchable circularly polarized luminescence. *Nat. Commun.* **12**, 6320 (2021).

21. Oki, O., *et al.* Robust Angular Anisotropy of Circularly Polarized Luminescence from a Single Twisted-Bipolar Polymeric Microsphere. *J. Am. Chem. Soc.* **143**, 8772-8779 (2021).
22. Li, P. & Deng, J. Switchable Chiroptical Flexible Films Based on Chiral Helical Superstructure: Handedness Inversion and Dissymmetric Adjustability by Stretching. *Adv. Funct. Mater*. **31**, 2105315 (2021).
23. Gu, L., *et al.* Circularly Polarized Organic Room Temperature Phosphorescence from Amorphous Copolymers. *J. Am. Chem. Soc.* **143**, 18527-18535 (2021).
24. Garain, S., Sarkar, S., Chandra Garain, B., Pati, S.K. & George, S.J. Chiral Arylene Diimide Phosphors: Circularly Polarized Ambient Phosphorescence from Bischromophoric Pyromellitic Diimides. *Angew. Chem. Int. Ed.* **61**, e202115773 (2022).
25. Xu, C., Yin, C., Wu, W. & Ma, X. Tunable room-temperature phosphorescence and circularly polarized luminescence encoding helical supramolecular polymer. *Sci. China Chem.* **65**, 75-81 (2021).
26. Hirata, S. & Vacha, M. Circularly Polarized Persistent Room-Temperature Phosphorescence from Metal-Free Chiral Aromatics in Air. *J. Phys. Chem. Lett.* **7**, 1539-1545 (2016).
27. Liang, X., *et al.* Organic Room-Temperature Phosphorescence with Strong Circularly Polarized Luminescence Based on Paracyclophanes. *Angew. Chem. Int. Ed.* **58**, 17220-17225 (2019).
28. Li, H., *et al.* Stimuli-Responsive Circularly Polarized Organic Ultralong Room Temperature Phosphorescence. *Angew. Chem. Int. Ed.* **59**, 4756-4762 (2020).
29. Liu, R., Ding, B., Liu, D. & Ma, X. Switchable circularly polarized Room-Temperature phosphorescence based on pure organic amorphous binaphthyl polymer. *Chem. Eng. J.* **421**, 129732 (2021).
30. Gong, Z.-L., *et al.* Frontiers in circularly polarized luminescence: molecular design, self-assembly, nanomaterials, and applications. *Sci. China Chem.* **64**, 2060-2104 (2021).
31. Yue, B. & Zhu, L. Dynamic Modulation of Supramolecular Chirality Driven by Factors from Internal to External Levels. *Chem. Asian J.* **14**, 2172-2180 (2019).
32. Yao, L., *et al.* Circularly Polarized Luminescence from Chiral Tetranuclear Copper(I) Iodide Clusters. *J. Phys. Chem. Lett.* **11**, 1255-1260 (2020).
33. Wang, C., *et al.* Photo-Induced Dynamic Room Temperature Phosphorescence Based on Triphenyl Phosphonium Containing Polymers. *Adv. Funct. Mater.* **32**, 2111941 (2022).
34. Zang, L.X., Shao, W.H., Kwon, M.S., Zhang, Z.G. & Kim, J. Photoresponsive Luminescence Switching of Metal-Free Organic Phosphors Doped Polymer Matrices. *Adv. Optical Mater.* **8**, 2000654 (2020).
35. Gmelch, M., Thomas, H., Fries, F. & Reineke, S. Programmable transparent organic luminescent tags. *Sci. Adv.* **5**, eaau7310 (2019).
36. Zhang, G., Palmer, G.M., Dewhirst, M.W. & Fraser, C.L. A dual-emissive-materials design concept enables tumour hypoxia imaging. *Nat. Mater.* **8**, 747-751 (2009).
37. Ma, L., Sun, S., Ding, B., Ma, X. & Tian, H. Highly Efficient Room-Temperature Phosphorescence Based on Single-Benzene Structure Molecules and Photoactivated Luminescence with Afterglow. *Adv. Funct. Mater.* **31**, 2010659 (2021).
38. Kwon, M.S., Lee, D., Seo, S., Jung, J. & Kim, J. Tailoring intermolecular interactions for efficient room-temperature phosphorescence from purely organic materials in amorphous polymer matrices. *Angew. Chem. Int. Ed.* **53**, 11177-11181 (2014).

39. Zhao, B., Pan, K. & Deng, J. Combining Chiral Helical Polymer with Achiral Luminophores for Generating Full-Color, On–Off, and Switchable Circularly Polarized Luminescence. *Macromolecules* **52**, 376-384 (2018).
40. Rizzo, P., Abbate, S., Longhi, G. & Guerra, G. Circularly polarized luminescence of syndiotactic polystyrene. *Opt. Mater.* **73**, 595-601 (2017).
41. Zhao, B., Yu, H., Pan, K., Tan, Z. & Deng, J. Multifarious Chiral Nanoarchitectures Serving as Handed-Selective Fluorescence Filters for Generating Full-Color Circularly Polarized Luminescence. *ACS Nano* **14**, 3208-3218 (2020).

Supporting Information

1. Synthesis

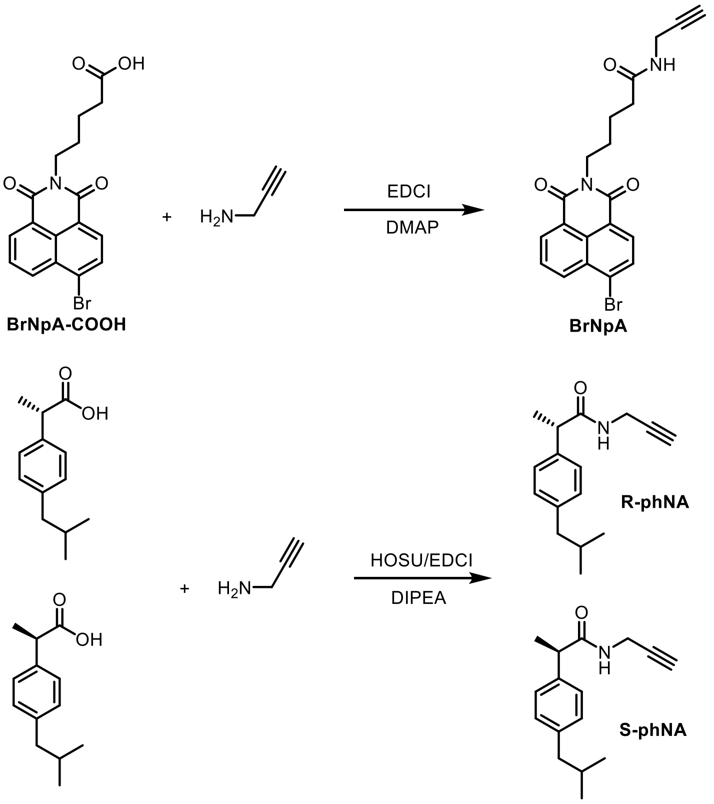

Figure S1. Synthetic routes of monomer.

(R)/(S)-2-(4-isobutylphenyl)-N-(prop-2-yn-1-yl)propenamide (*R/S*-phNA): (R)/(S)-2-(4-isobutylphenyl)propanoic acid (100 mg, 0.49 mmol, 1 eq), N-Hydroxy succinimide (HOSU) (67 mg, 0.582 mmol, 1.2 eq) and EDC·HCl (111.5 mg, 0.582 mmol, 1.2 eq) in DCM (100 ml). After the reaction mixture was stirred for 30 min, mono-Propargylamine (32 mg, 0.582 mmol, 1.2eq) and *N,N*-Diisopropylethylamine (DIPEA) (188 mg, 1.45 mol, 3 eq) was added to the above solution. The reaction mixture was stirred overnight at room temperature. The reaction was quenched with water, extracted with DCM, dried over $MgSO_4$, filtered, concentrated, and purified by column chromatography on silica (DCM: EA = 30:1) to give white solid 86 mg. Yield: 66.3%. ^{1}H NMR (400 MHz, Chloroform-*d*) δ 7.19 (d, *J* = 8.2 Hz, 2H), 7.13 (d, *J* = 8.1 Hz, 2H), 5.51 (s, 1H), 4.09 – 3.88 (m, 2H), 3.55 (q, *J* = 7.2 Hz, 1H), 2.46 (d, *J* = 7.2 Hz, 2H), 2.17 (t, *J* = 2.5 Hz, 1H), 1.93 – 1.78 (m, 1H), 1.52 (d, *J* = 7.3 Hz, 3H), 0.90 (d, *J* = 6.6 Hz, 6H). HRMS (ESI) m/z: $[M + Na]^+$ calculated for $C_{16}H_{21}NNaO^+$, 266.1515; found, 266.1521.

5-(6-bromo-1,3-dioxo-1H-benzo[de]isoquinolin-2(3H)-yl)-N-(prop-2-yn-1-yl)pentanamide (BrNpA): A mixture of **BrNpA-COOH** (100 mg, 0.27 mmol, 1eq), mono-Propargylamine (17.8 mg, 0.32 mmol, 1.2 eq), EDC·HCl (61.3 mg, 0.32 mmol, 1.2 eq), and DMAP (39.1 mg, 0.32 mmol, 1.2 eq) in DCM (100 ml) was stirred at rt for 5 h, quenched with aqueous water, extracted with DCM, dried over $MgSO_4$, filtered, concentrated, and purified by column chromatography on silica (DCM: EA = 1:1) to give white solid 78 mg. Yield: 79.3%. ^{1}H NMR (400 MHz, Chloroform-*d*) δ 8.66 (dd, *J* = 7.3, 1.2 Hz, 1H), 8.58 (dd, *J* = 8.5, 1.1 Hz, 1H), 8.42 (d, *J* = 7.8 Hz, 1H), 8.05 (d, *J* = 7.8 Hz, 1H), 7.86 (dd, *J* = 8.5, 7.3 Hz, 1H), 5.94 (s, 1H), 4.21 (t, *J* = 6.8 Hz, 2H), 4.05 (dd, *J* = 5.2, 2.6 Hz, 2H), 2.33 (t, *J* = 7.1 Hz, 2H), 2.20 (t, *J* = 2.6 Hz, 1H), 1.83 – 1.72 (m, 4H). HRMS (ESI) m/z: $[M + Na]^+$ calculated for $C_{20}H_{17}BrN_2NaO_3^+$, 435.0315; found, 435.0320.

Synthesis of the Polymer p(phNA-co-BrNpA): According to the copolymerization molar ratio, the monomer R/S-phNA, BrNpA and the catalyst $(nbd)Rh^+B^-(C_6H_5)_4$ were dissolved in 2 mL of chloroform ($CHCl_3$). The polymerization was performed under the following conditions: [monomer]/[catalyst] =100, N_2 at 30 ^{0}C for 6 h. The resulting mixture was added into methanol to precipitate polymeric materials. The crude product was washed with methanol 2–3 times to give purified polymers.

Synthesis of the corresponding PMMA Films: The copolymers (10 mg), and PMMA (1 g) were dissolved in 10-20 mL $CHCl_3$ solution. The mixture was further stirred for 3 h to remove excess $CHCl_3$, and formed a homogenous dispersed solution. The solution was transferred to a template container, placed in air for 10 min, and then dried sequentially in a 40 °C oven for another 3 h. The transparent and flexible p(phNA-co-BrNpA)-PMMA film were obtained.

2. Characterization of the structure of monomer and copolymer

(R-phNA was picked out as the representative for the following elaboration.**)**

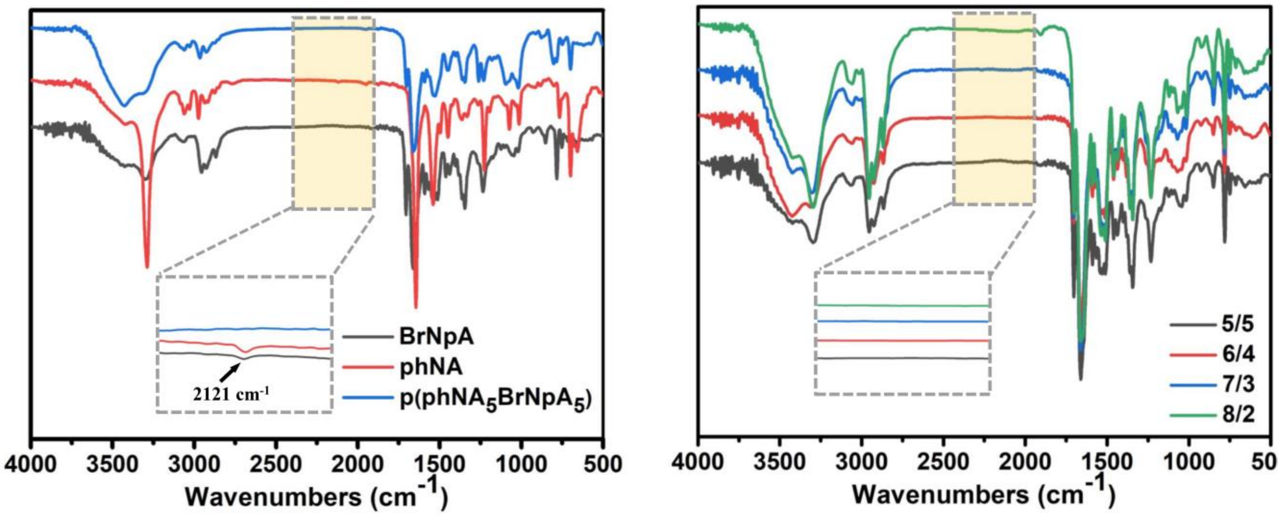

Figure S2. The FT-IR spectra of **phNA, BrNpA** and **p(phNA-co-BrNpA)** with different copolymerization molar ratios. (KBr tablet).

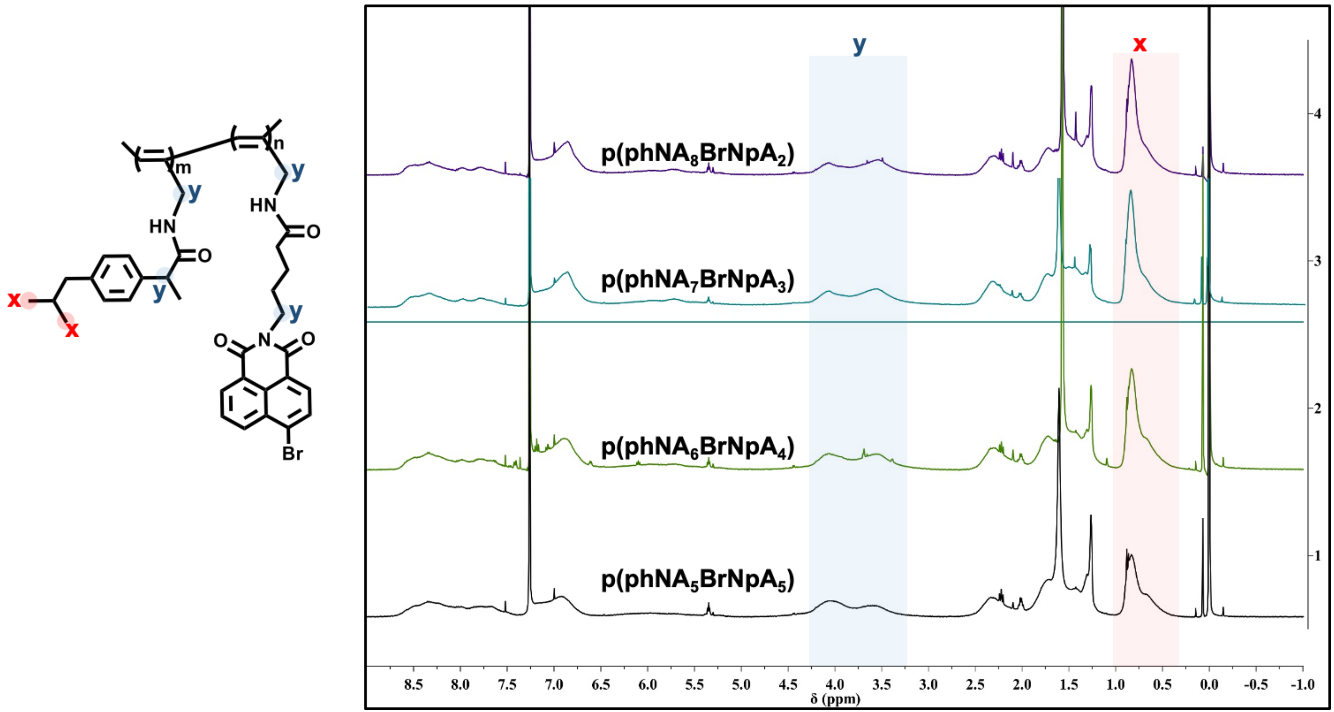

Figure S3. The Chemical structure and ^{1}H NMR spectra of the p(phNA-co-BrNpA).

Table S1. Polymer composition and properties of the synthesized copolymers.

polymer	**Composition (mol%)[a)]**	**Mn[b)]**	**Mw[b)]**	**D[b)]**
p(phNA$_5$BrNpA$_5$)	5:4.41	29262	49724	1.699
p(phNA$_6$BrNpA$_4$)	6:3.81	20829	37538	1.802
p(phNA$_7$BrNpA$_3$)	7:3.64	25978	71627	2.757
p(phNA$_8$BrNpA$_2$)	8:2.82	21173	55391	2.616

[a)] Proportions of **phNA** and **BrNpA** in the copolymers as determined by ^{1}H NMR (Figure S3) spectroscopy.
[b)] Determined by GPC.

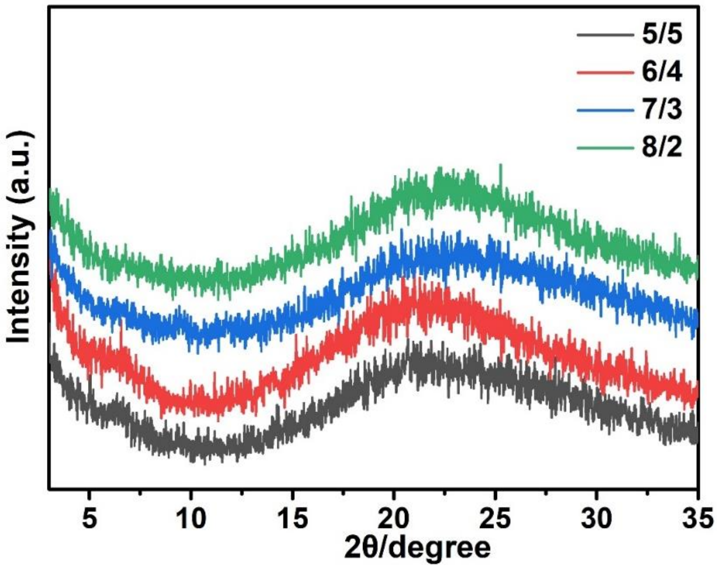

Figure S4. The XRD patterns of **p(phNA-co-BrNpA)** with different copolymerization molar ratios.

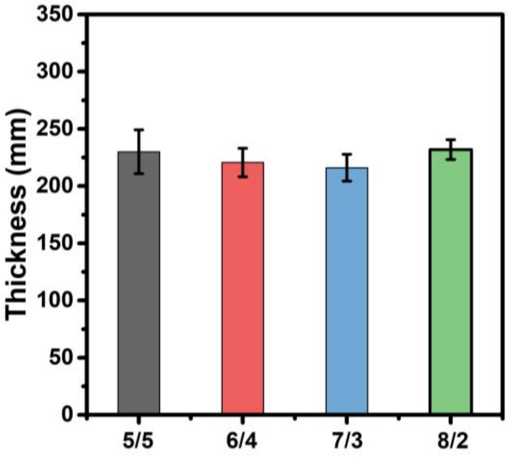

Figure S5. The thickness of the **p(phNA-co-BrNpA)-PMMA** film.

3. Optical properties of the materials

(**R-phNA** was picked out as the representative for the following elaboration.)

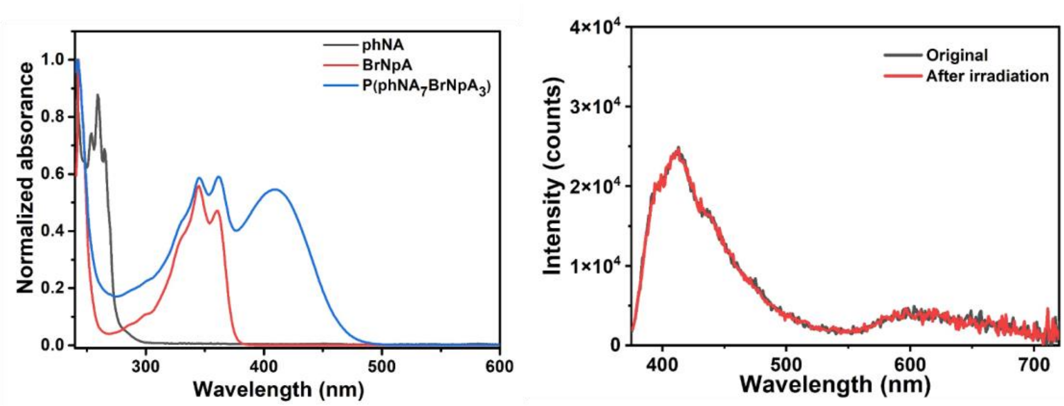

Figure S6. a) The normalized absorption spectra of **phNA, BrNpA** and **p(phNA$_7$BrNpA$_3$)**. b) The photoluminescence spectra of **p(phNA$_7$BrNpA$_3$).**

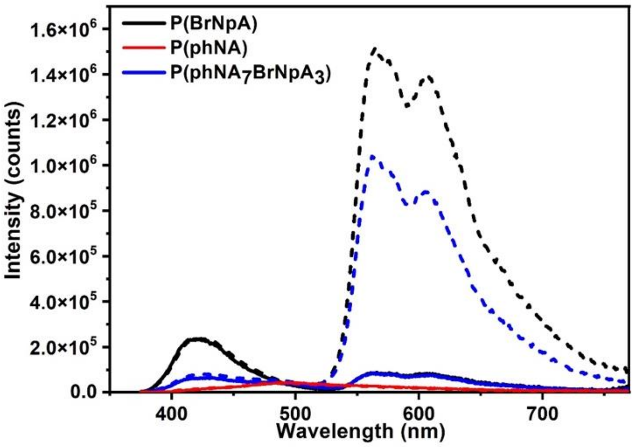

Figure S7. The photoluminescence spectra of **p(phNA)-PMMA, BrNpA-PMMA** and **p(phNA-co-BrNpA)-PMMA** film before (solid lines) and after (broken lines) continuous UV light irradiation.

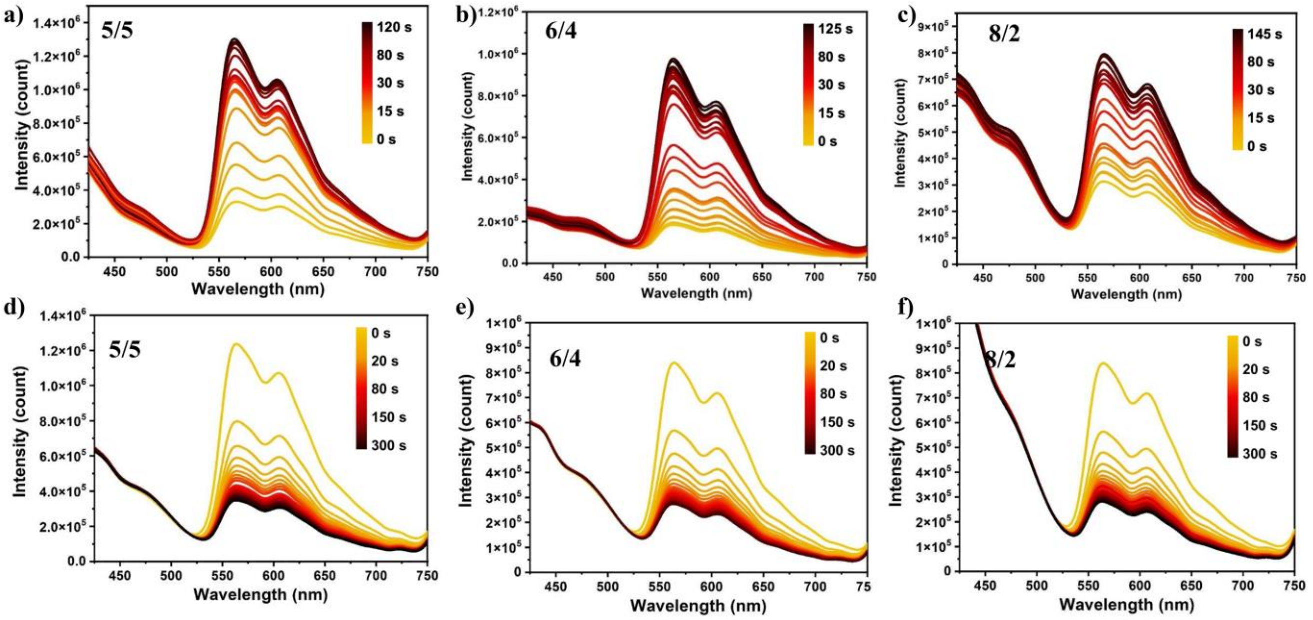

Figure S8. The photoluminescence spectra of **p(phNA-co-BrNpA)**-PMMA under a), b), c) sustaining UV light irradiation and d), e), f) after ceasing irradiation.

5. Chiro-optical properties of the materials

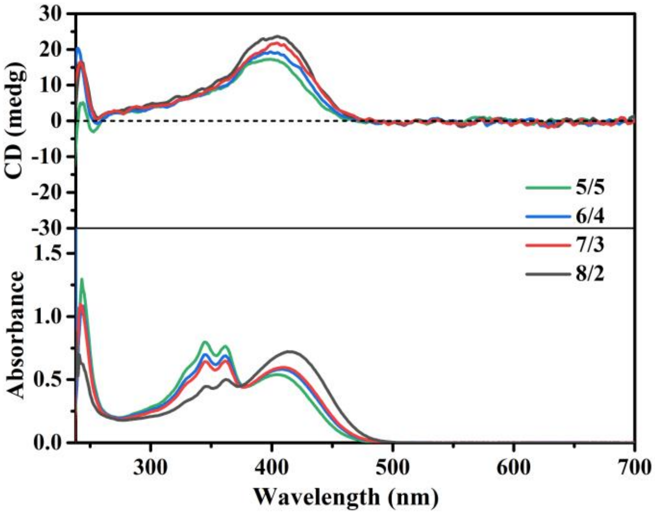

Figure S9. The CD spectra of **p(*S*-phNA-co-BrNpA)** with different copolymerization molar ratios in THF.

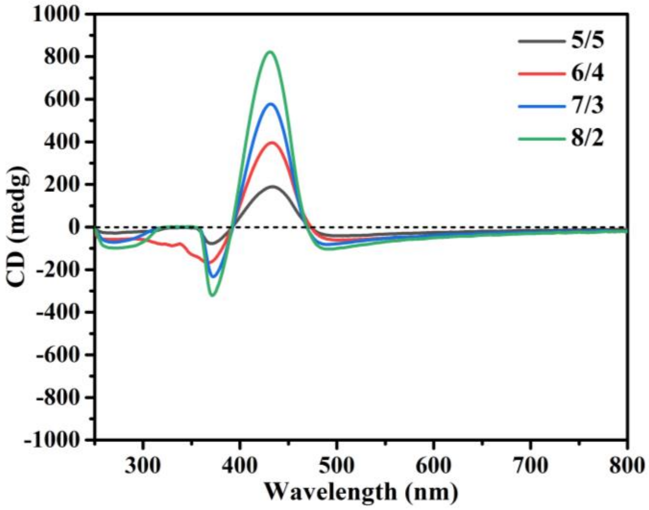

Figure S10. The CD spectra of **p(*S*-phNA-co-BrNpA)**-PMMA with different copolymerization molar ratios.

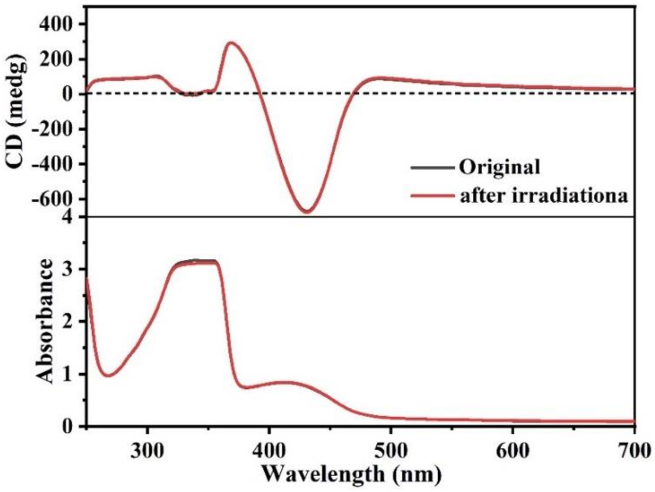

Figure S11. The CD spectra of **p(*R*-phNA$_7$BrNpA$_3$)**-PMMA before and after continuous UV light irradiation.

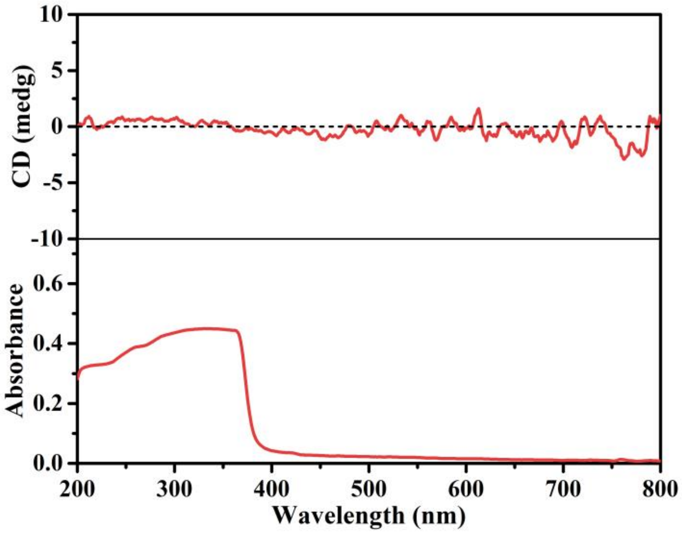

Figure S12. The CD spectra of p(**BrNpA)-**PMMA.

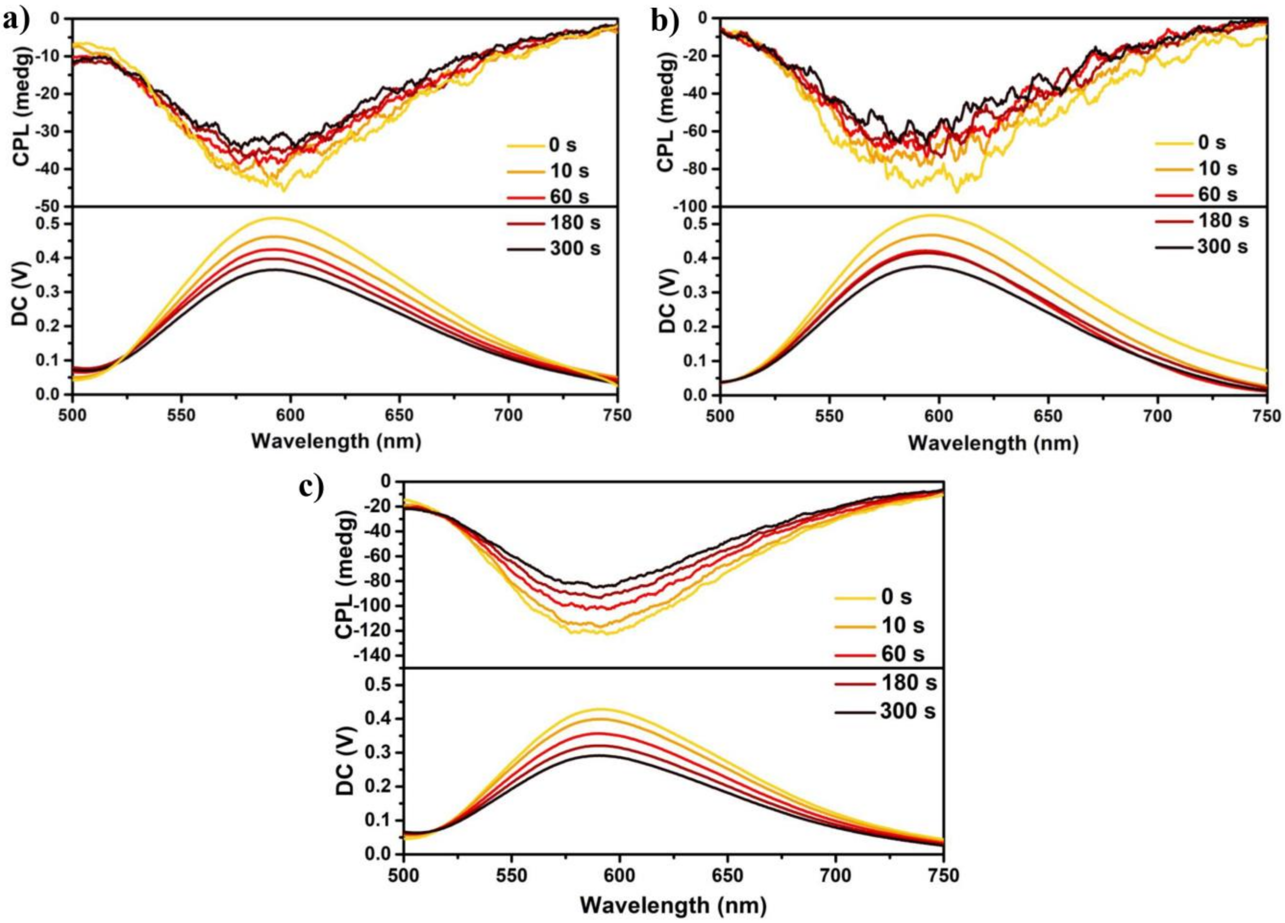

Figure S13. The CPL spectra of **p(R-phNA-co-BrNpA)-**PMMA with a) 5/5, b) 6/4, c) 8/2 copolymerization molar ratios.

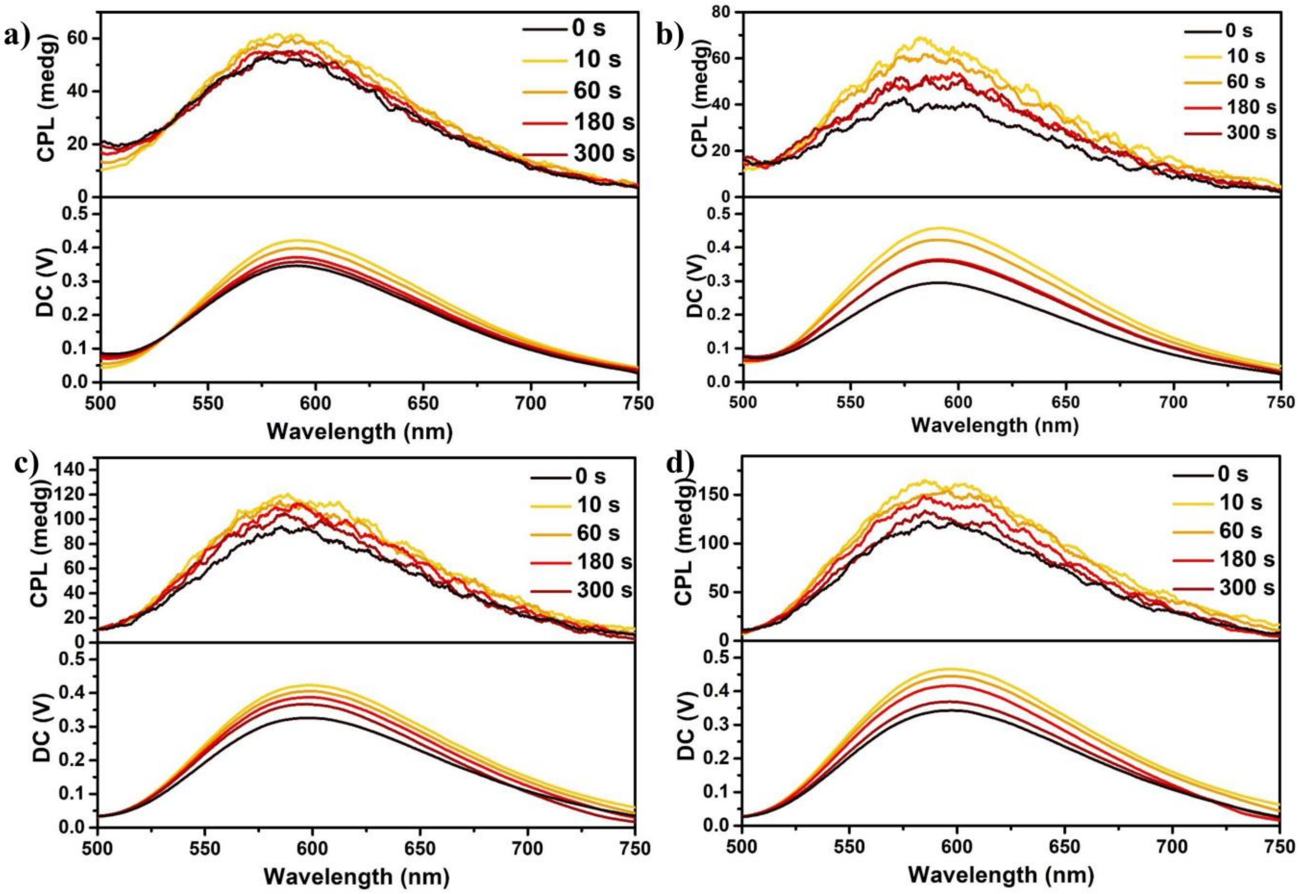

Figure S14. The CPL spectra of **p(*S*-phNA-co-BrNpA)**-PMMA with a) 5/5, b) 6/4, c) 7/3 d) 8/2 copolymerization molar ratios.

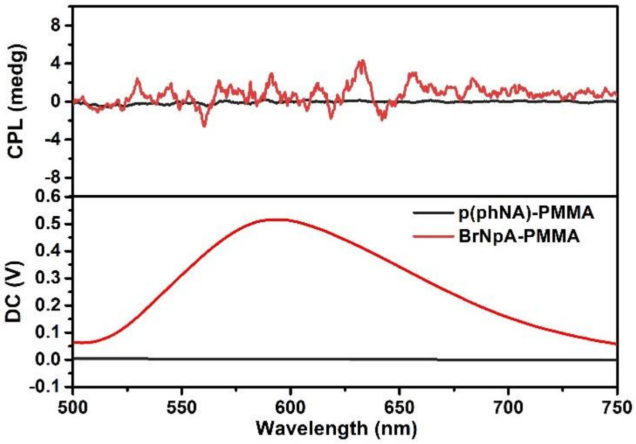

Figure S15. The CPL spectra of p(*S*-phNA)-PMMA, BrNpA-PMMA.

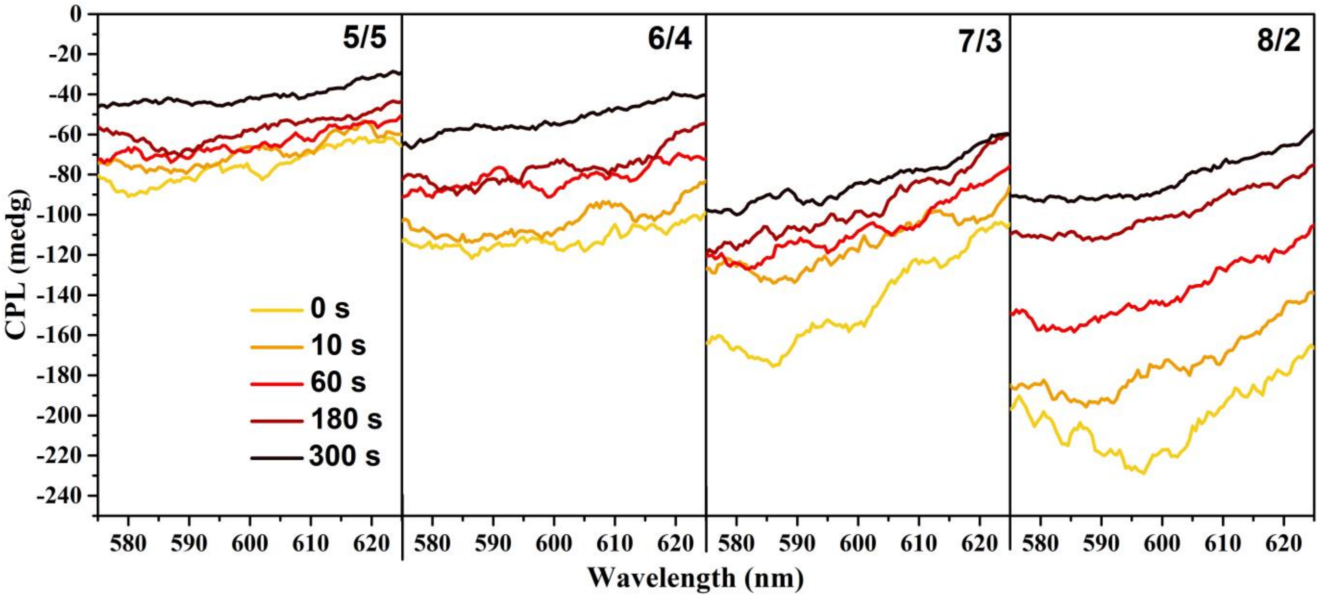

Figure S16. The CPL spectra of **p(*R*-phNA-co-BrNpA)**-PMMA with copolymerization molar ratios under high scanning speed.

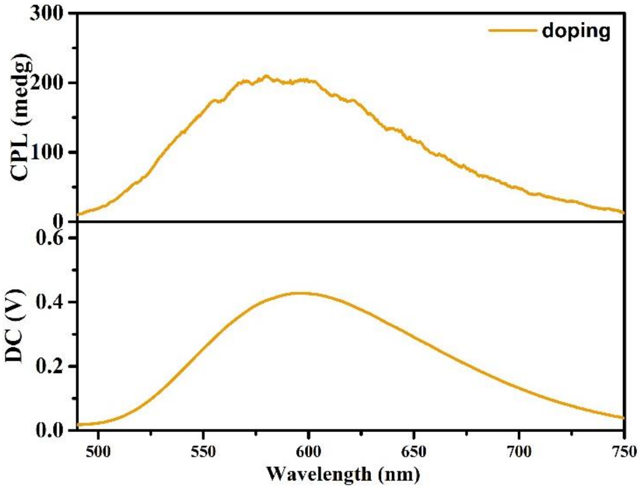

Figure S17. The CPL spectra of BrNpA doping in p(S-phNA)-PMMA.

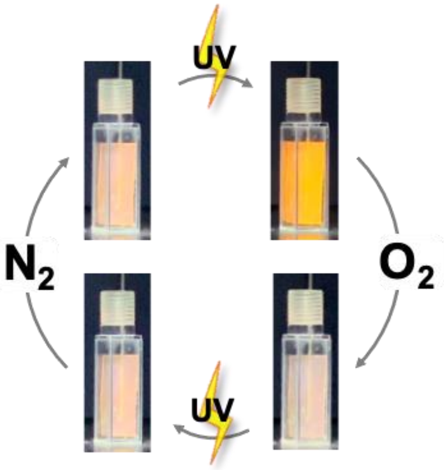

Figure S18. The photograph of nitrogen and oxygen alternately filling the quartz tube.

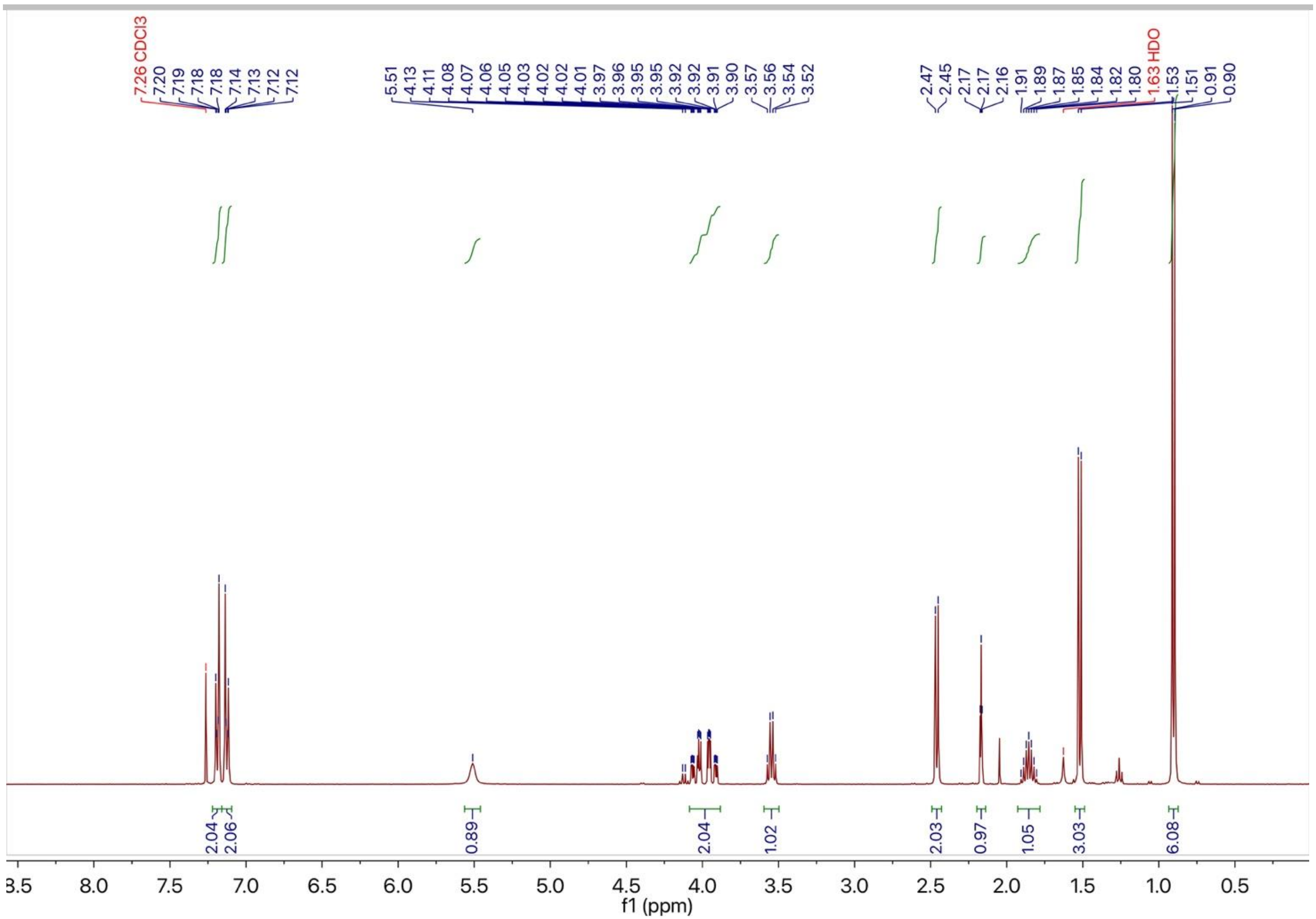

Figure S19. ^{1}H NMR spectrum (400 MHz) of ***R*-phNA** in $CDCl_3$.

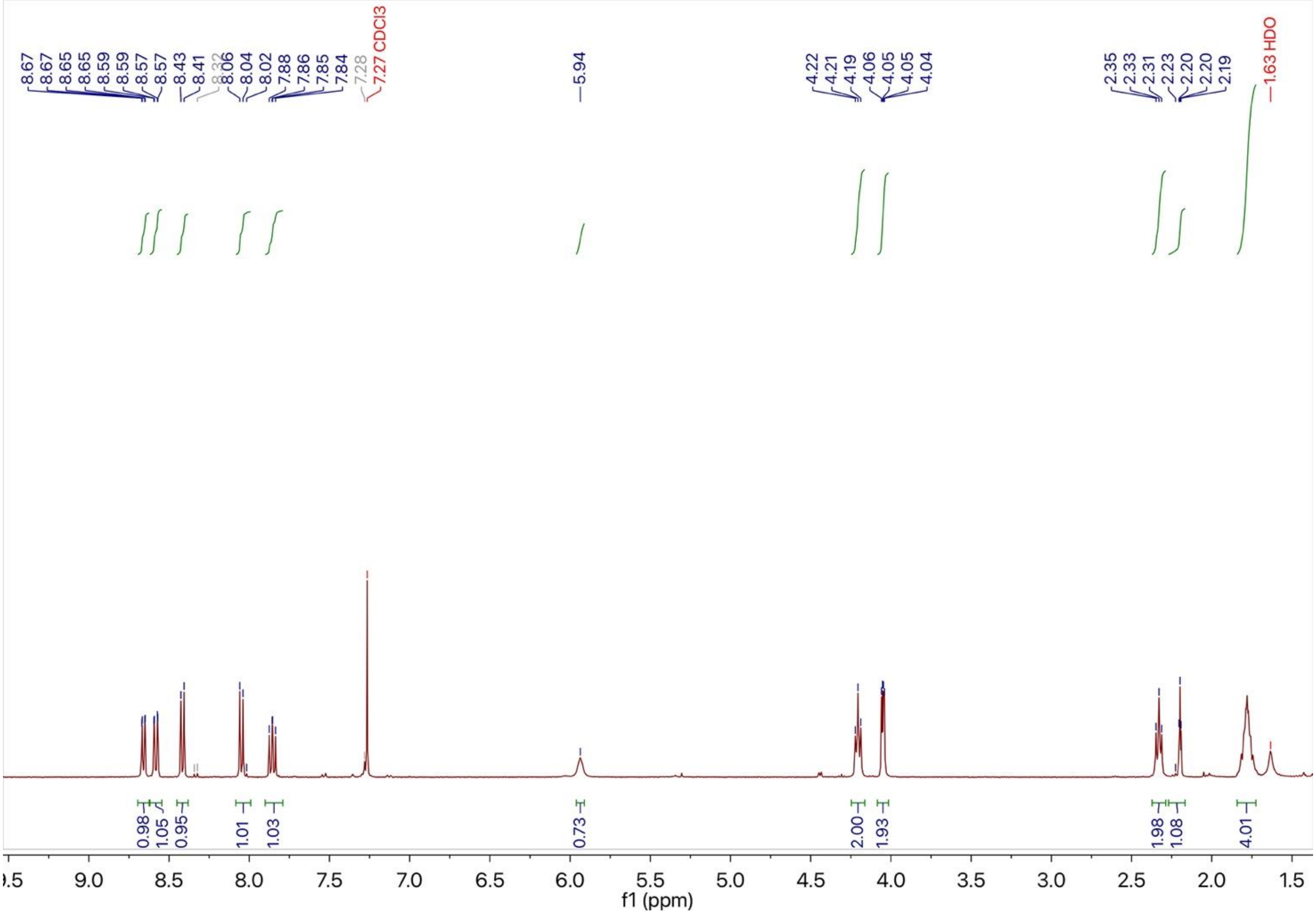

Figure S20. ^{1}H NMR spectrum (400 MHz) of **BrNpA** in $CDCl_3$.

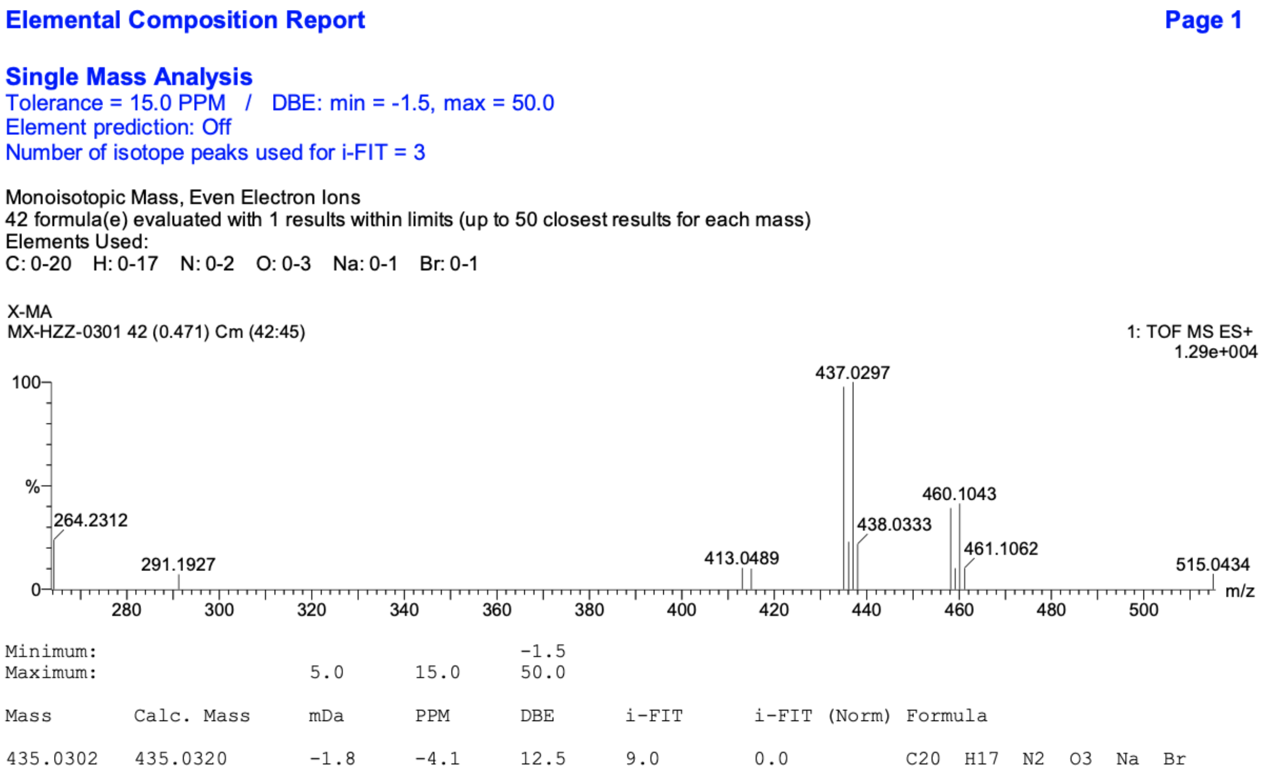

Elemental Composition Report **Page 1**

Single Mass Analysis
Tolerance = 15.0 PPM / DBE: min = -1.5, max = 50.0
Element prediction: Off
Number of isotope peaks used for i-FIT = 3

Monoisotopic Mass, Even Electron Ions
42 formula(e) evaluated with 1 results within limits (up to 50 closest results for each mass)
Elements Used:
C: 0-20 H: 0-17 N: 0-2 O: 0-3 Na: 0-1 Br: 0-1

X-MA
MX-HZZ-0301 42 (0.471) Cm (42:45)

```
Minimum:                                      -1.5
Maximum:                   5.0       15.0     50.0

Mass       Calc. Mass      mDa       PPM      DBE       i-FIT       i-FIT (Norm) Formula

435.0302   435.0320        -1.8      -4.1     12.5      9.0         0.0          C20  H17  N2  O3  Na  Br
```

Figure S21. HRMS (ESI) spectrum of **BrNpA**.

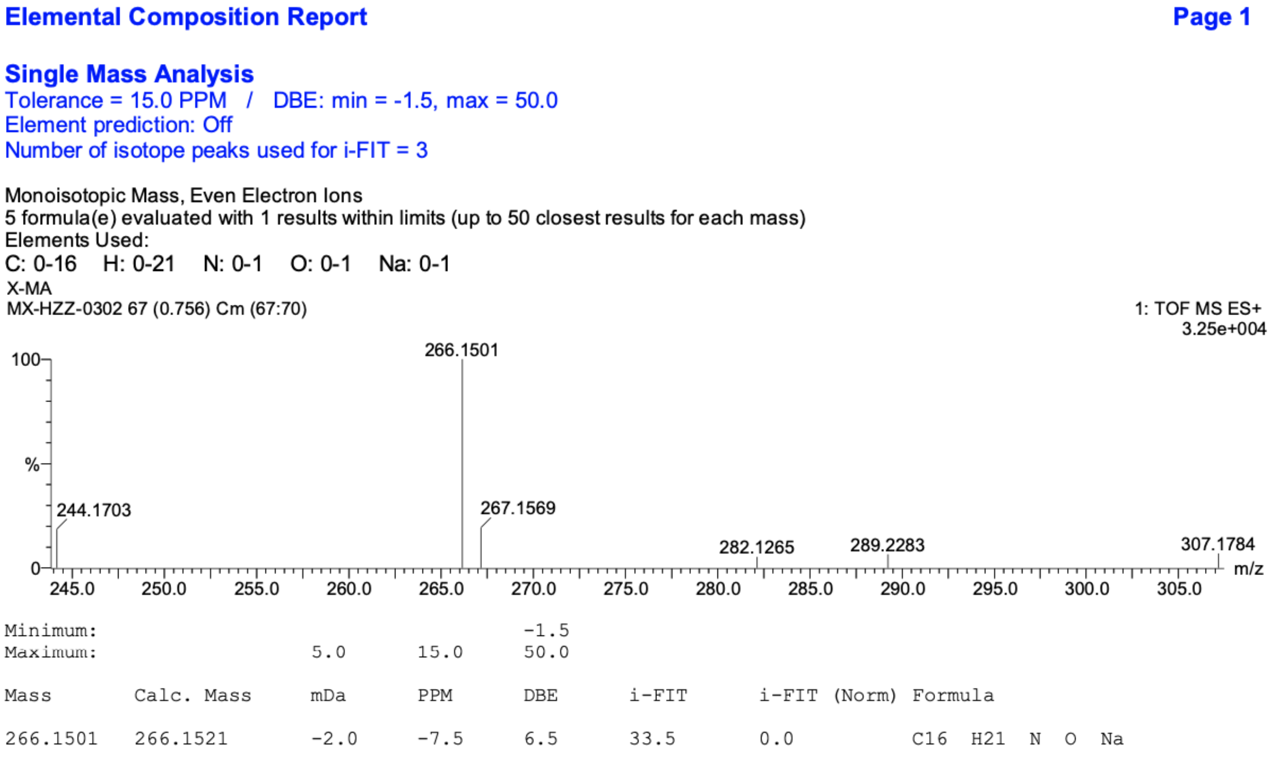

Elemental Composition Report **Page 1**

Single Mass Analysis
Tolerance = 15.0 PPM / DBE: min = -1.5, max = 50.0
Element prediction: Off
Number of isotope peaks used for i-FIT = 3

Monoisotopic Mass, Even Electron Ions
5 formula(e) evaluated with 1 results within limits (up to 50 closest results for each mass)
Elements Used:
C: 0-16 H: 0-21 N: 0-1 O: 0-1 Na: 0-1
X-MA
MX-HZZ-0302 67 (0.756) Cm (67:70)

```
Minimum:                                      -1.5
Maximum:                   5.0       15.0     50.0

Mass       Calc. Mass      mDa       PPM      DBE       i-FIT       i-FIT (Norm) Formula

266.1501   266.1521        -2.0      -7.5     6.5       33.5        0.0          C16  H21  N  O  Na
```

Figure S22. HRMS (ESI) spectrum of **R-phNA**.